Phase diagrams of the triangular Ising antiferromagnet-variational approximations

1981 J. Phys. A: Math. Gen. 14 2767

(http://iopscience.iop.org/0305-4470/14/10/028)

J. Phys. A: Math. Gen. **14** (1981) 2767–2777. Printed in Great Britain

Phase diagrams of the triangular Ising antiferromagnet variational approximations

A Malakis†

Institutt for Teoretisk Fysikk, University of Trondheim, 7034 Trondheim-NTH, Norway

Received 13 April 1981

Abstract. We derive an appropriate generalisation of Baxter's variational method and define a sequence of variational approximations for 'antiferromagnetic' models on the triangular lattice. Expressions for the sublattice magnetisations are derived from a variational principle for the partition function per site. We apply the method to the triangular antiferromagnet and obtain approximate phase diagrams in the temperature–field and temperature–magnetisation (density) planes.

1. Introduction

In 1968 Baxter developed a sequence of variational approximations for the monomer–dimer problem on the square lattice. This method was generalised to the Potts model (Kelland 1976) and to the square IRF (interactions-round-a-face) model with row and column reversal symmetry (Baxter 1978). In this latter generalisation, Baxter gave a graphical interpretation of the essential ingredients of these approximations, the 'corner', 'half-row' and 'half-column' transfer matrices. He showed also that the matrix equations defining the variational approximations can be given a graphical interpretation that enables one to avoid the tedious algebraic manipulations by which these approximations are derived.

Recently the method has been applied to obtain the first 23 terms in the low-temperature expansion of the square Ising model in a field (Baxter and Enting 1979), the first 24 terms of the high-density series for hard squares (Baxter *et al* 1980) and the entropy of hard hexagons (Baxter and Tsang 1980). A general feature borne out from these studies is that the approximations are quantitatively very good even when the dimension of the matrices is quite small. The approximations tend to the exact results as the size of the matrices tends to infinity (Baxter 1977, Tsang 1977).

In this paper we present the generalisation of the variational method for 'antiferromagnetic' models on the triangular lattice, i.e. models for which the lattice symmetry is broken at low temperatures. The matrix equations and their graphical interpretation will be given in the following section. In § 3 we derive the variational expression for the partition function per site, from which the magnetisation is obtained. A numerical procedure for solving the equations will be described in § 4. As an application we obtain, in § 5, phase diagrams for the triangular antiferromagnet in an external field.

† Present address: University of Athens, Division of Mechanics, Panepistimiopolis, Athens 621, Greece.

0305-4470/81/102767+11$01.50

2. Variational approximations for the triangular antiferromagnet

Consider an Ising spin system (spin variables $\sigma_i = \pm 1$, for brevity $\sigma_i = \pm$) on a triangular lattice with N sites for which the partition function can be written

$$Z_N = \sum_{\{\sigma\}} \prod_{(i,j,k)} w(\sigma_i, \sigma_j, \sigma_k) \tag{1}$$

where each triplet (i, j, k) in (1) surrounds an elementary triangle and $w(\sigma_i, \sigma_j, \sigma_k)$ is the Boltzmann weight of the interacting spin triplet $(\sigma_i, \sigma_j, \sigma_k)$. The summation in (1) is over all 2^N spin configurations on the triangular lattice and the product extends over all elementary triangles (i, j, k). Furthermore, we consider interactions for which the Boltzmann factor $w(a, b, c)$ is unchanged by permuting a, b, c. The most general interaction of this form gives

$$w(a, b, c) = \exp\{(k_B T)^{-1}[\tfrac{1}{6}H(a+b+c) + \tfrac{1}{2}J_2(ab+bc+ac) + J_3 abc]\}. \tag{2}$$

The partition function per site in the thermodynamic limit is

$$k = \lim_{N\to\infty} Z_N^{1/N}. \tag{3}$$

In order to describe the triangular antiferromagnet with these interactions, one would have to divide the lattice into three sublattices (sublattices 1, 2 and 3). However, since significant fluctuations occur between one of these sublattices (say, sublattice 3) and the other two (sublattices 1 and 2), we shall only distinguish between sites on sublattice 3 (defining a sublattice L') and sites on sublattices 1 or 2 (defining a sublattice L). Alternatively, we could derive the equations without identifying sublattices 1 and 2 and then note that the equations permit solutions for which sublattices 1 and 2 are identified. This distinction between sublattices is dictated from the ground-state properties of the system; for certain values of H, J_2, J_3 the system admits a ground state with spins on one sublattice down (-1) and on the other two up $(+1)$.

Let the sites on L be denoted by filled circles and the sites on L' by open circles. With the 'corner' segment in figure 1(a) we associate two 2^n by 2^n matrices $A(+)$ and $A(-)$. The spin variable a of $A(a)$ is associated with the corner site of segment 1(a) which is a site of sublattice L (filled circle). The first index of $A(a)$, say $\lambda \equiv \{\lambda_1, \lambda_2, \ldots, \lambda_n\}$; $\lambda_i = \pm$, is associated with the spin configurations along the side $\lambda_1\lambda_2 \ldots \lambda_n$ of segment 1(a) so that λ_1 corresponds to a site on L, λ_2 to a site on L' and so on. The second index of $A(a)$, $\mu \equiv \{\mu_1, \mu_2, \ldots, \mu_n\}$, is associated with side $\mu_1\mu_2 \ldots \mu_n$ of segment 1(a) so

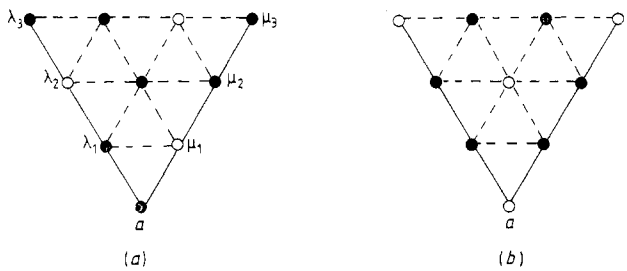

Figure 1. Lattice (corner) segments corresponding respectively to the matrices $A(a)$ and $B(a)$ (for $n = 3$).

that μ_1 corresponds to a site on L', μ_2 and μ_3 to sites on L and so on. The element $A_{\lambda\mu}(a)$ of $A(a)$ is the combined Boltzmann weight of segment $1(a)$, summed over all interior spins. With the 'corner' segment in figure $1(b)$ we associate two 2^n by 2^n matrices $B(a)$ (the spin variable a of $B(a)$ is now associated with a site on L', open circle). From figure $1(b)$ one can see that the matrices B are invariant under transposition

$$B(a) = B^{\mathrm{T}}(a). \tag{4}$$

Similarly eight 2^n by 2^n matrices $F(a, b)$ and $G(a, b)$ $(a, b = \pm)$ are associated with the 'half-row' segments in figures $2(a)$ and $2(b)$ respectively (both spin variables a and b of F as well as the first spin variable of $G(a, b)$ are associated with sites on L, whereas the second spin variable b of $G(a, b)$ is associated with a site on L'). Again it is easily seen that

$$F(a, b) = F^{\mathrm{T}}(b, a). \tag{5}$$

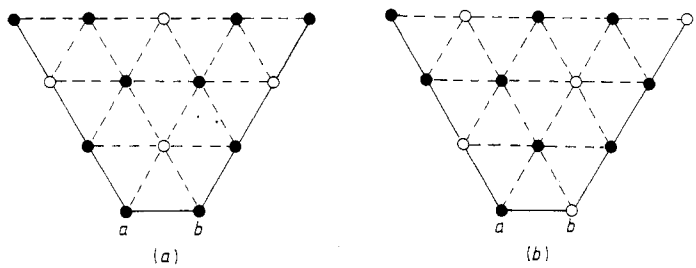

Figure 2. Lattice segments for the matrices $F(a, b)$ and $G(a, b)$ respectively.

Generalising the two graphical equations of Baxter and Tsang (1980) for the ferromagnetic n . n model, we obtain for the present case six graphical equations shown in figures 3 and 4; their matrix equations are given below as equations (6) and (7):

$$\sum_b F(a, b)A(b)A^{\mathrm{T}}(b)F(b, a) = \xi_1\{A(a)A^{\mathrm{T}}(a)\}^2 \tag{6a}$$

$$\sum_b G^{\mathrm{T}}(b, a)A^{\mathrm{T}}(b)A(b)G(b, a) = \xi_2 B^4(a) \tag{6b}$$

$$\sum_b G(a, b)B^2(b)G^{\mathrm{T}}(a, b) = \xi_3\{A^{\mathrm{T}}(a)A(a)\}^2 \tag{6c}$$

$$\sum_c w(a, b, c)F(a, c)A(c)G(c, b) = \eta_1^{1/2}A(a)G(a, b)B(b) \tag{7a}$$

$$\sum_c w(a, b, c)G(a, c)B(c)G^{\mathrm{T}}(b, c) = \eta_3^{1/2}A^{\mathrm{T}}(a)F(a, b)A(b). \tag{7b}$$

Equations $(6a)$, $(6b)$ and $(6c)$ correspond to the graphical equations in figures $3(a)$, $3(b)$ and $3(c)$ respectively; figures $4(a)$ and $4(b)$ give the same equation, namely equation $(7a)$ with $\eta_1 = \eta_2$. Finally, equation $(7b)$ corresponds to the graphical equation of figure

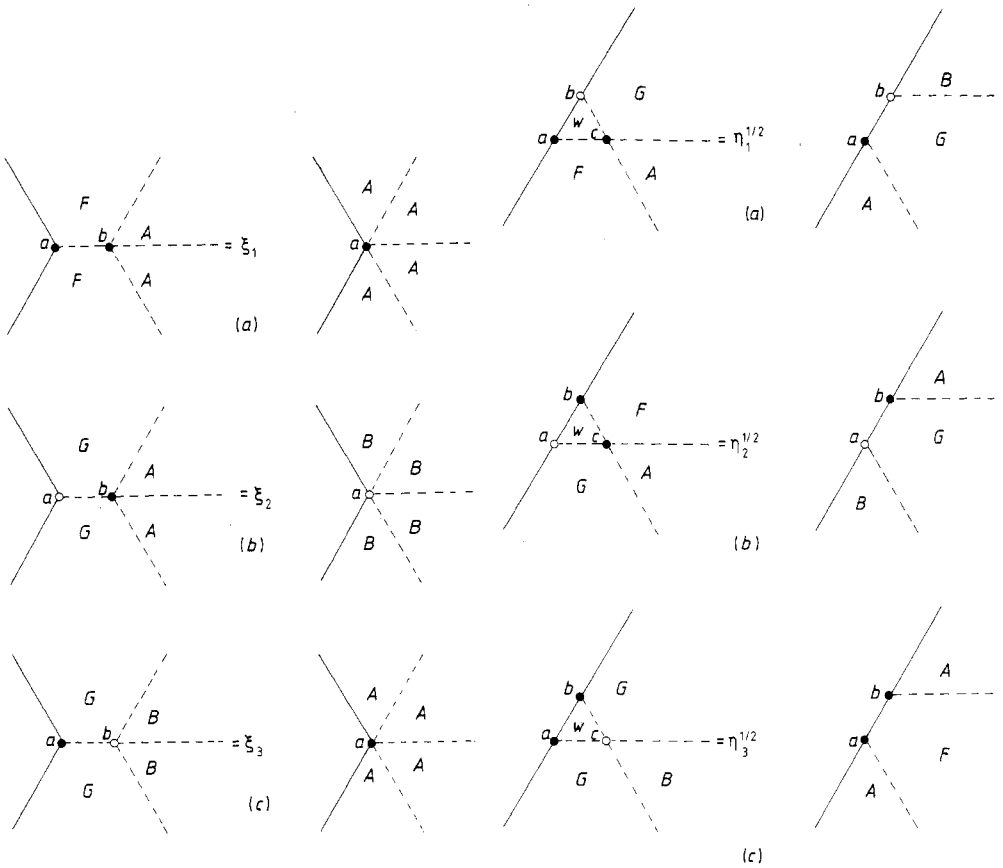

Figure 3. Graphical equations corresponding respectively to equations (6*a*), (6*b*) and (6*c*). One may read these equations clockwise or anticlockwise.

Figure 4. Both graphical equations (4*a*) and (4*b*) correspond to equation (7*a*) (read (4*a*) anticlockwise to obtain (7*a*), read (4*b*) clockwise and interchange *a* and *b* to obtain (7*a*)). Finally, (4*c*) corresponds to equation (7*b*) (read anticlockwise to obtain (7*b*), if one reads clockwise the transpose of (7*b*) is obtained).

4(*c*). The partition function per site is given in terms of the factors ξ_1, ξ_2, ξ_3, η_1, η_2 and η_3 by

$$k = \{(\eta_1\eta_2\eta_3)/(\xi_1\xi_2\xi_3)\}^{1/3} \qquad \eta_1 = \eta_2. \tag{8}$$

Using an argument similar to that given by Baxter and Tsang (1980) (see also Baxter *et al* 1980) we can clarify equation (8): Each graphical equation in figures 3 (4) states that the unnormalised probability distribution of the spins on the left of the LHS is the same, to within a normalisation factor ξ ($\eta^{1/2}$), with the unnormalised probability distribution of the spins on the left of the RHS. Normalisation of these probability distributions will affect the factors ξ and η but not the ratio $(\eta_1\eta_2\eta_3)/(\xi_1\xi_2\xi_3)$. There are $2n+1$ $(n+1)$ more sites on the LHS than on the RHS in each graphical equation 3 (4), hence, three more sites contribute to the numerator than to the denominator of $(\eta_1\eta_2\eta_3)/(\xi_1\xi_2\xi_3)$. When n is large each extra site contributes a factor k, so that equation (8) is satisfied.

It may be remarked that equation (6*c*) can be obtained by post-multiplying equation (7*b*) by $A^{\mathrm{T}}(b)F(b, a)$, summing over b and then using the transpose of equation (7*a*) on the LHS and equation (6*a*) on the RHS . Identifying the resulting equation with equation (6*c*), we find

$$\xi_3 = (\eta_3^{1/2}/\eta_1^{1/2})\xi_1. \tag{9}$$

It also follows that in order to solve the equations we can use only one of (6*a*) and (6*c*). Thus, equations (6*b*), (6*c*), (7*a*) and (7*b*) define the matrices A, B, G and F to within normalisation factors. By fixing the normalisation of these matrices, ξ_2, ξ_3, η_1 and η_3 are determined and hence k is obtained from (8) and (9).

3. Magnetisations

In this section we give a variational expression for the partition function per site and derive expressions for the sublattice magnetisations. Let us define:

$$r_1 = \sum_a \mathrm{Tr}\{(A^{\mathrm{T}}(a)A(a))^3\} \tag{10a}$$

$$r_2 = \sum_{ab} \mathrm{Tr}\{A^{\mathrm{T}}(a)F(a, b)A(b)A^{\mathrm{T}}(b)F(b, a)A(a)\} \tag{10b}$$

$$r_3 = \sum_a \mathrm{Tr}\{B^6(a)\} \tag{10c}$$

$$r_4 = \sum_{ab} \mathrm{Tr}\{A(a)G(a, b)B^2(b)G^{\mathrm{T}}(a, b)A^{\mathrm{T}}(a)\} \tag{10d}$$

$$r_5 = \sum_{abc} w(a, b, c)\,\mathrm{Tr}\{G(a, c)B(c)G^{\mathrm{T}}(b, c)A^{\mathrm{T}}(b)F(b, a)A(a)\}. \tag{10e}$$

It is easily verified from (6), (7) and (10) that:

$$\xi_1 = r_2/r_1 \qquad \xi_2 = r_4/r_3 \qquad \xi_3 = r_4/r_1 \tag{11a}$$

$$\eta_1^{1/2} = \eta_2^{1/2} = r_5/r_4 \qquad \eta_3^{1/2} = r_5/r_2. \tag{11b}$$

For instance the first of (11*a*) is obtained by post-multiplying (6*a*) by $A(a)A^{\mathrm{T}}(a)$, summing over a, taking traces and using (10*a*) and (10*b*). The partition function per site, equation (8), can then be expressed in terms of the r, namely

$$k = (r_1^{2/3}r_3^{1/3}r_5^2)/(r_2r_4^2). \tag{12}$$

The RHS of (12) is stationary in A, B, F and G (as one can easily verify by differentiating with respect to the elements of these matrices); it follows that (12) is a variational expression for k.

The magnetisation per site, M, is obtained using the thermodynamic formula

$$M = k_{\mathrm{B}}T\partial(\ln k)/\partial H. \tag{13}$$

The derivative of k with respect to H is evaluated from (12), considering A, B, F and G as constants since this expression is stationary in these matrices. After some algebraic

manipulations we find (using (6), (7) and (10)):

$$M = \tfrac{2}{3}m + \tfrac{1}{3}m' \tag{14}$$

$$m = \frac{\Sigma_a\, a\ \mathrm{Tr}\{(A^{\mathrm{T}}(a)A(a))^3\}}{\Sigma_a\ \mathrm{Tr}\{(A^{\mathrm{T}}(a)A(a))^3\}} \tag{15}$$

$$m' = \frac{\Sigma_a\, a\ \mathrm{Tr}\{B^6(a)\}}{\Sigma_a\ \mathrm{Tr}\{B^6(a)\}}. \tag{16}$$

Expressions (15) and (16) can also be given a straightforward graphical interpretation (see Baxter and Tsang 1980). m and m' are identified as the sublattice magnetisations corresponding to sublattices L and L'.

4. Numerical procedure

Equations (6) and (7) can be solved by the Newton–Raphson method, or any other method for solving systems of nonlinear equations. However, initial guesses are required in any such method. Baxter (1978) has described an iterative procedure for solving similar equations in the non-critical region. The main virtue of his method is that it can be used to obtain reasonable initial guesses in a systematic way; these guesses can then be used to solve the equations by the Newton–Raphson method. We therefore proceed to adapt his method to the present model.

Let us define

$$\tilde{G}(a, b) = A(a)G(a, b) \tag{17a}$$

$$\tilde{A}(a) = A(a)A^{\mathrm{T}}(a). \tag{17b}$$

Using (17a) and (17b) one can rewrite equations (6) and (7) in terms of $\tilde{A}$, B, F and $\tilde{G}$. Furthermore, it is easily verified that our equations are invariant under the transformations

$$\tilde{A}(a) \to R(a)\tilde{A}(a)R^{\mathrm{T}}(a) \qquad B(a) \to Q(a)B(a)Q^{\mathrm{T}}(a) \tag{18a}$$

$$F(a, b) \to R(a)F(a, b)R^{\mathrm{T}}(b) \qquad \tilde{G}(a, b) \to R(a)\tilde{G}(a, b)Q^{\mathrm{T}}(b) \tag{18b}$$

$R(a)$ and $Q(a)$ being orthogonal matrices. It follows that one can use a representation in which $B(a)$ and $\tilde{A}(a)$ are diagonal. However, for the procedure given below only the diagonal property of $B(a)$ is essential, although for convenience we shall also consider $\tilde{A}(a)$ to be diagonal. Let us further define two 2^{n+1} by 2^{n+1} matrices $U(b)$ and two 2^{n+1} by 2^n matrices $E(b)$ by:

$$U(b) = \begin{pmatrix} w(+, b, +)F(+, +) & w(+, b, -)F(+, -) \\ w(-, b, +)F(-, +) & w(-, b, -)F(-, -) \end{pmatrix} \tag{19a}$$

and

$$E(b) = \xi_2^{1/2}\begin{pmatrix} \tilde{G}(+, b)B^{-2}(b) \\ \tilde{G}(-, b)B^{-2}(b) \end{pmatrix}. \tag{19b}$$

Using these, equations (7a) and (6b) can be written as

$$U(b)E(b) = \eta_1^{1/2}E(b)B(b) \tag{20a}$$

$$E^{\mathrm{T}}(b)E(b) = I. \tag{20b}$$

Since $B(b)$ is diagonal equation (20a) implies that each column j of $E(b)$ is an eigenvector of $U(b)$ with eigenvalue $\eta_1^{1/2}B_{jj}(b)$. Equation (20b) states that the eigenvectors of the symmetric matrices $U(b)$ should be chosen orthonormal. Defining also a 2^{n+1} by 2^{n+1} matrix S by

$$S = (E(+)E(-))\begin{pmatrix} B^3(+) & 0 \\ 0 & B^3(-) \end{pmatrix} \tag{21}$$

we find, using (6c) and the diagonal property of $\tilde{A}$,

$$\tilde{A}^3_{ii}(+) = (\xi_2/\xi_3)(SS^{\mathrm{T}})_{ii} \qquad i = 1, 2, \ldots, 2^n \tag{22a}$$

$$\tilde{A}^3_{ii}(-) = (\xi_2/\xi_3)(SS^{\mathrm{T}})_{jj} \qquad i = 1, 2, \ldots, 2^n \qquad j = 2^n + i. \tag{22b}$$

The matrices $F(a, b)$ can be determined from (7b), i.e.

$$F(a, b) = \eta_3^{1/2}\tilde{A}^{-1}(a)\Big(\sum_c w(a, b, c)\tilde{G}(a, c)B(c)\tilde{G}^{\mathrm{T}}(b, c)\Big)\tilde{A}^{-1}(b). \tag{23}$$

Although the natural sequence of these approximations is to take the matrices $\tilde{A}$, B, F and $\tilde{G}$ as 2^n by 2^n ($n = 0, 1, \ldots$), it has been found in previous studies (see for instance, Baxter and Tsang 1980) that this is not necessary. We shall therefore define the $n_1 \times n_2$ approximation as follows: $\tilde{A}(+)$, $B(+)$, $F(+, +)$ and $\tilde{G}(+, +)$ are $n_1 \times n_1$; $F(+, -)$ and $G(+, -)(F(-, +)$ and $\tilde{G}(-, +))$ are $n_1 \times n_2$ ($n_2 \times n_1$); $\tilde{A}(-)$, $B(-)$, $F(-, -)$ and $\tilde{G}(-, -)$ are $n_2 \times n_2$; $\tilde{A}(-)$ and $B(-)$ are $n_2 \times n_2$ matrices. The numerical procedure can now be outlined as follows.

(i) Give some initial values to $F(+, +)$, $F(+, -)$ and $F(-, -)$. From (19a) determine $U(-)$ and $U(+)$ and obtain their eigenvalues in decreasing order and the corresponding orthonormal eigenvectors.

(ii) For each value of b, $-(+)$, there are $2n_2$ ($2n_1$) eigenvalues. Select the n_2 (n_1) first eigenvalues of $U(-)(U(+))$ and their eigenvectors.

(iii) Fix the normalisation of B (i.e. $B_{11}(-) = 1$) to obtain $\eta_1^{1/2}$ and hence identify the diagonal elements of $B(-)$ ($B(+)$) with the first n_2 (n_1) eigenvalues of $U(-)$ ($U(+)$) divided by $\eta_1^{1/2}$.

(iv) Fix the normalisation of $\tilde{G}$ (i.e. $\tilde{G}_{11}(+, -) = 1$) and thus using the selected eigenvectors and (19b) obtain ξ_2 and $\tilde{G}(a, b)$.

(v) Fix the normalisation of $\tilde{A}$ (i.e. $\tilde{A}_{11}(+) = 1$) and using (22) obtain ξ_3 and $\tilde{A}(b)$.

(vi) Fix the normalisation of F (i.e. $F_{11}(+, +) = 1$) to obtain η_3 and $F(a, b)$ from (23).

Having now new values for the matrices $F(a, b)$ one can go to step (i) and repeat, until sufficient numerical accuracy is achieved. As has been pointed out by Baxter and Tsang (1980) such procedures can be also used to obtain initial guesses for higher approximations by keeping in step (ii) more eigenvalues and eigenvectors and modifying n_2 (n_1) accordingly.

The normalisation of B, $\tilde{A}$, F and $\tilde{G}$ is dictated by numerical convenience. The choice given in the parentheses above is found convenient for nearest-neighbour antiferromagnetic interactions in weak fields, for example.

5. Phase diagrams of the triangular antiferromagnet

We consider the triangular antiferromagnet ($J_3 = 0$, $J_2 < 0$; also we take $H \geq 0$, since the $H \leq 0$ case follows by symmetry) and obtain phase diagrams in the (T^*, H^*)

($T^* = k_B T/|J_2|$; $H^* = H/|J_2|$) and in the (T^*, ρ) ($\rho = (1-M)/2$ is the density of particles) planes. This model is interesting from both theoretical and experimental points of view (Fisher 1967). In particular, its lattice gas equivalent provides a reasonable description for absorbed systems like helium or krypton on graphite (Ostlund and Berker 1979).

In zero field, the model is exactly soluble (Houtappel 1950) and there is no transition at any finite temperature, due to the infinite degeneracy of the ground state (Wannier 1950). With the application of a field $H^* < 6$, the ground state is triply degenerate, i.e. there exist three equivalent ordered configurations. Such a ground-state configuration has all spins on one sublattice (say L') down (-1) and all spins on the other two sublattices (defining L) up ($+1$). At 'low temperatures' there exists an *antiferromagnetic phase* in which two of the sublattice magnetisations are equal to one another but different from the third. At some 'higher temperature' a transition occurs to a *paramagnetic phase* in which the three sublattice magnetisations are equal to each other. It was first suggested by Domb (1960) that the two phases are separated on the (T^*, H^*) plane by a line of critical points running from the critical field at zero temperature to the origin. Qualitatively, this phase diagram is now well understood, since its two 'end-points' are known and its slope at the critical field is related to the critical activity z_c of the hard-hexagon model (recently solved by Baxter (1980)) by

$$\lambda = \left.\frac{dT^*}{dH^*}\right|_{H^*=6} = -2/\ln z_c = -2/\ln\{\tfrac{1}{2}(11+5\sqrt{5})\} = -0.831\ldots. \tag{24}$$

Furthermore, from symmetry and scaling arguments it is expected (Kinzel and Schick 1981) that the slope of the phase diagram at zero field ($dT^*/dH^*|_{H^*=0}$) is infinite.

Quantitatively the phase boundary is less well known and there have been several attempts to estimate it (Burley 1965, Metcalf 1973, Schick *et al* 1977, Kinzel and Schick 1981, Dóczi-Réger and Hemmer 1981). Such estimates can be obtained from the variational approximations. In the paramagnetic region the solution of equations (6) and (7) is expected to satisfy the symmetry properties

$$A(a) = A^{\mathrm{T}}(a) = B(a) \tag{25a}$$

$$G(a, b) = F(a, b) \tag{25b}$$

$$\xi_1 = \xi_2 = \xi_3 \qquad \eta_1 = \eta_3 \tag{25c}$$

$$M = m = m' \tag{25d}$$

and our equations reduce to those of Baxter and Tsang (1980). Therefore, we search for two physically interesting solutions, the paramagnetic solution (satisfying (25)) and the antiferromagnetic solution (not satisfying (25)). Within an approximation, each of these solutions exists in the region where it maximises k, but also a little outside this region. The two solutions give, in general, different values (where they both exist) for the partition function per site, k_p and k_a respectively. Thus, we can determine the phase boundary by the condition $k_p = k_a$ (in the paramagnetic region $k_p > k_a$, whereas in the antiferromagnetic region $k_a > k_p$).

The 1×1 and 2×1 approximations for the phase boundary are shown in figure 5(a), together with the Kikuchi approximation. The 1×1 approximation may be considered as equivalent to the Kramers–Wannier approximation (Kramers and Wannier 1941, Baxter 1978) and is comparable in accuracy to the Kikuchi approximation. It can be seen from figure 5(a) that the variational approximations (as well as the mean-field and

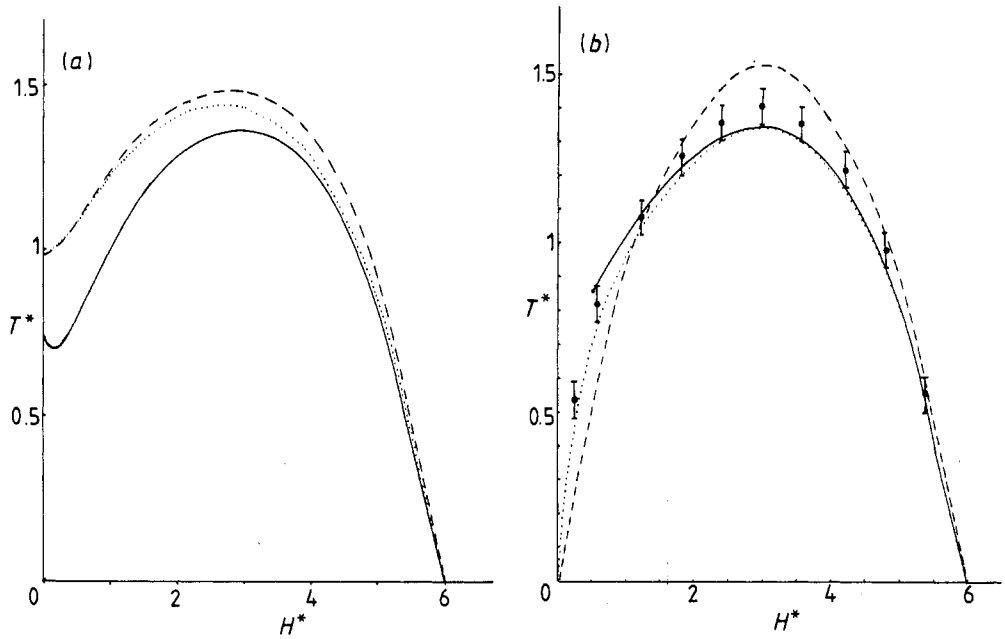

Figure 5. Phase diagrams of the triangular Ising antiferromagnet in temperature–field plane. (*a*) Full curve, this work: 2×1 approximation; broken curve, this work: 1×1 approximation; dotted curve, Burley (1965): Kikuchi approximation. (*b*) Full curve, this work: accurate part of the 3×2 approximation; broken curve, Dóczi-Réger and Hemmer (1981): interface approximation; dotted curve, Kinzel and Schick (1981): 'phenomenological–Nightingale' approximation; points, Metcalf (1973): Monte Carlo.

Kikuchi approximations) fail to reproduce the exact zero-field result. However, the 2×1 approximation shows that the trend of the variational approximations is correct, but the shape of the phase diagram in weak fields is rather peculiar. As a result of this deficiency we have not been able to obtain accurate estimates near zero field. The numerical results for the 2×1, 2×2 and 3×2 approximations are given in table 1. The

Table 1.

	2×1 approximation		2×2 approximation		3×2 approximation	
H^*	T^*	M_a	T^*	M_a	T^*	M_a
0.5	0.796	0.117	0.857	0.095	0.857	0.094
1	1.007	0.183	1.015	0.176	1.015	0.176
1.5	1.170	0.227	1.167	0.226	1.166	0.226
2	1.280	0.264	1.275	0.264	1.272	0.264
2.5	1.346	0.296	1.338	0.296	1.333	0.297
3	1.364	0.326	1.357	0.326	1.348	0.326
3.5	1.333	0.355	1.328	0.354	1.315	0.353
4	1.244	0.384	1.241	0.383	1.225	0.378
4.5	1.083	0.412	1.081	0.411	1.061	0.402
5	0.817	0.435	0.817	0.435	0.795	0.422
5.5	0.428	0.444	0.428	0.444	0.414	0.428

values of the slope λ predicted by the 2×2 and 3×2 approximations are $\lambda_{2\times2}=-0.857\ldots$ and $\lambda_{3\times2}=-0.829\ldots$, in good agreement with the exact value (24). Apparently, the critical temperatures given in table 1 for the 3×2 approximation are accurate to the second decimal place (for $H^*=1, 2$ and 3 this was verified using the 3×3 and 4×3 approximations). Figure 5(*b*) shows the accurate part of the phase diagram obtained from the 3×2 approximation and those obtained by the interface method of Müller-Hartmann and Zittartz (1977) (Dóczi-Réger and Hemmer 1981), the phenomenological scaling approach of Nightingale (1976) (Kinzel and Schick 1981) and the Monte Carlo calculation (Metcalf 1973). The comparison favours the '3×2' and the 'phenomenological' diagrams, in particular for $H^*>3$ where their agreement is excellent.

Regarding the nature of phase transitions the variational approximations give, in general, first-order transitions with jumps in magnetisation. These jumps are small in magnitude and tend to zero in higher approximations, so that the $\infty\times\infty$ solution of equations (6) and (7) would yield, as expected, second-order transitions. At the critical points the magnetisation of the antiferromagnetic solution M_a (given in table 1) is more accurate than that of the paramagnetic solution. The limiting value of the critical magnetisation as we approach the critical field ($H_c^*=+6$) follows from the critical density of the hard-hexagon lattice gas (Baxter 1980)

$$M_c=1-2\rho_c=0.447\ldots \qquad (\rho_c=(5-\sqrt{5})/10=0.276\ldots). \tag{26}$$

The 2×2 and 3×2 variational approximations yield $M_c\sim0.44$ and $M_c\sim0.43$ respectively, in good agreement with (26). The limiting value (26) determines one 'end-point' (i.e. $(0, M_c)$) of the (T^*, M) phase diagram. The other 'end-point' is not known, but it is expected (Kinzel and Schick 1981) to be the origin (0, 0). The corresponding 'end-points' on the (T^*, ρ) plane are: $(0, \rho_c)$ and (0, 0.5). In figure 6 the 2×2 approximation for the (T^*, ρ) phase diagram is shown together with the phenomenological approximation. Again only in the region corresponding to fields $H^*<3$ do they differ

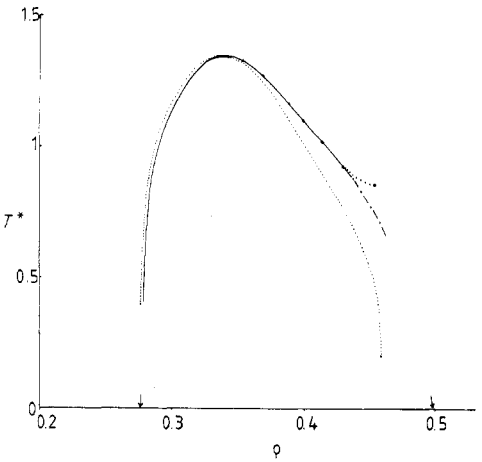

Figure 6. Phase diagram of the triangular lattice gas in temperature-density plane. The dotted curve shows the 'phenomenological–Nightingale' approximation of Kinzel and Schick (1981). The full curve corresponds to the 2×2 approximation (table 1); the dotted part indicates the region where the approximation becomes inaccurate; the chain part shows a possible extrapolation.

significantly. As pointed out by Kinzel and Schick (1981) the phenomenological approach has difficulties near zero field; it yields a finite slope for the (T^*, H^*) diagram and a non-zero critical magnetisation as we approach zero field. On the other hand, the variational approximations are expected to converge (as $n_1, n_2 \to \infty$) to the exact values, but near zero field they do so in a rather curious fashion (see figure 5(*a*)). From figures 5(*b*) and 6, it can be seen that the deviations of the 'variational diagrams' from the 'phenomenological diagrams' are consistent with the predictions of infinite slope and zero critical magnetisation at zero field. Apparently, for $0.5 < H^* < 3$ the 'variational diagrams' are more accurate than the 'phenomenological diagrams'.

In summary, we have presented a generalisation of Baxter's variational method and utilised it to obtain the phase diagrams of the triangular antiferromagnet. Away from zero field the diagrams are accurate and for $H^* > 3$ they are in excellent agreement with those of the phenomenological method.

Acknowledgments

I should like to express my gratitude to Professor P C Hemmer for many useful discussions and constructive suggestions. I am also grateful for the hospitality of the Institutt for teoretisk fysikk, NTH, University of Trondheim, and to NTNF for a fellowship.

References

Baxter R J 1968 *J. Math. Phys.* **9** 650–4
—— 1977 *J. Stat. Phys.* **17** 1–14
—— 1978 *J. Stat. Phys.* **19** 461–78
—— 1980 *J. Phys. A: Math. Gen.* **13** L61–70
Baxter R J and Enting I G 1979 *J. Stat. Phys.* **21** 103–23
Baxter R J, Enting I G and Tsang S K 1980 *J. Stat. Phys.* **22** 465–89
Baxter R J and Tsang S K 1980 *J. Phys. A: Math. Gen.* **13** 1023–30
Burley D M 1965 *Proc. Phys. Soc.* **85** 1163–72
Dóczi-Réger J and Hemmer P C 1981 to be published
Domb C 1960 *Phil. Mag. Suppl.* **9** 149–361
Fisher M E 1967 *Rep. Prog. Phys.* **30** 615
Houtappel R M F 1950 *Physica* **16** 425
Kelland S B 1976 *Can. J. Phys.* **54** 1621–6
Kinzel W and Schick M 1981 to be published
Kramers H A and Wannier G H 1941 *Phys. Rev.* **60** 263
Metcalf B D 1973 *Phys. Lett.* **45A** 1–2
Müller-Hartmann E and Zittartz J 1977 *Z. Phys.* B **27** 261
Nightingale M P 1976 *Physica* A **83** 561
Ostlund S and Berker A N 1979 *Phys. Rev. Lett.* **42** 843
Schick M, Walker J S and Wortis M 1977 *Phys. Rev.* B **16** 2205–19
Tsang S K 1977 *J. Stat. Phys.* **17** 137–52
Wannier G H 1950 *Phys. Rev.* **79** 357–64